

Hydrodynamic pairing of vesicles in a confined flow

O. Aouane,^{1,2,3,*} A. Farutin,^{1,2} M. Thiébaud,^{1,2}

A. Benyoussef,⁴ C. Wagner,³ and C. Misbah^{1,2}

¹*Université Grenoble Alpes, LIPHY, F-38000, Grenoble, France*

²*CNRS, LIPHY, F-38000, Grenoble, France*

³*Experimental Physics, Saarland University, 66123 Saarbrücken, Germany.*

⁴*LMPHE, URAC 12, Faculté des Sciences,
Université Mohammed V- Agdal, Rabat, Morocco*

(Dated: September 12, 2022)

Abstract

The hydrodynamics-induced pairing mechanism of deformable closed bilayer membranes (vesicles, a model for red blood cells) is studied numerically with a special attention paid to the role of the confinement (the vesicles are within two rigid walls). This study unveils the complexity of the pairing mechanism due to hydrodynamic interactions. At weak confinement we find that two vesicles attract each other and form a stable pair if their initial distance is below a certain value. If the initial distance is beyond that distance, the vesicles repel each other and adopt a larger stable interdistance. This means that for the same confinement we have (at least) two stable branches and whether one branch prevails over the other depends only on initial conditions. An unstable branch is found between these two stable branches. At a critical confinement the stable branch corresponding to the smallest interdistance merges together with the unstable branch in the form of a saddle-node bifurcation. At this critical confinement we have a finite jump from a solution corresponding to an unbounded case to a solution which is induced by the presence of walls. The results are summarized in a complex phase diagram.

PACS numbers: 47.11.Hj, 47.15.G-, 83.50.Ha, 83.80.Lz, 87.16.D-

* Current address: Forschungszentrum Jülich GmbH, Helmholtz-Institute Erlangen-Nürnberg for Renewable Energy (IEK-11), Dynamics of Complex Fluids and Interfaces, Fürther Straße 248, 90429 Nürnberg, Germany

I. INTRODUCTION:

In the microcirculation, it is often observed that the red blood cells (RBCs) flow in single or multiple files forming small trains of cells, called clusters[1, 2]. The arrangement and organization of the RBCs depend on the diameter of the vessel and their concentration (hematocrit). Each RBC interacts hydrodynamically with the other cells[3]. RBCs can also interact via another mechanism, namely an interaction mediated by plasma proteins. The latter interaction is materialized either by bridging between RBCs or by a depletion force. In the bridging mechanisms proteins make a real bridge between two neighboring RBCs, while in the depletion mechanism osmosis is responsible for the cluster formation. We have recently discussed the implication of plasma proteins in the formation of RBC clusters in microcirculation [4]. The main objective is to gain further insight into the role of each mechanism. Therefore this paper will be directed towards numerical simulation in the presence of pure hydrodynamic interaction.

Several studies have been devoted to understanding the hydrodynamical interaction between suspended particles in the Stokes regime. Analytical models [5, 6] considered the motion of a linear array of rigid spheres at low Reynolds number in a cylindrical tube under a pressure-driven flow (i.e., an imposed Poiseuille flow). Wang and Skalak[5] estimated the hydrodynamic interaction's range between the spherical particles to be of the order of the tube diameter. Leichtberg *et al.*[6] showed that the interparticle interactions were relatively small at low confinements, reached a maximum at intermediate confinement, and were quickly damped out at high confinement. More recently, colloidal particles confined between two parallel plates in a quasi 2D geometry have been studied experimentally and theoretically [7–9]. The complexity in these systems arises from the difficulty to decouple the effect of Brownian diffusion from hydrodynamic interactions. An antidrag between the moving particles attributed to a negative hydrodynamic coupling has been reported. A change of sign of the hydrodynamic coupling (from attraction to repulsion) in a cylindrical channel was also observed [7]. The effect of boundaries on the hydrodynamic interactions has been studied in the case of water-in-oil droplets in quasi-1D microfluidic devices having a square section of the order of the size of the droplet, so that the droplets are constrained to move along the channel axis [10–12]. This study reported on a non-monotonous behavior

of the hydrodynamic interaction resulting from an interplay between the plug flow and the screening of the long-range hydrodynamic interaction induced by the confinement.

Janssen *et al.*[13] have studied numerically pairs of rigid spheres and deformable drops driven by a Poiseuille flow through a three-dimensional rectangular channel in the Stokes regime. Due to the reversibility of Stokes equations, the interdistance between a pair of rigid spheres does not evolve in time. However, for a pair of deformable drops, due to the upstream/down-stream shape asymmetry, hydrodynamics interaction leads to an attraction at large separation distances and repulsion at small interdistances. The long-range attraction was attributed to the source-quadrupole flows induced by droplets in the Hele-Shaw geometry. The pair of drops tends to the same stationary separation distance independently of the capillary number – a measure of the flow strength – which only affects the time needed to reach the stationary state.

Vesicles, a closed bilayer membrane of phospholipid molecules, have been used as a simplified model for RBCs to simulate blood flow in microcirculation [14, 16] with a focus on the role of the imposed flow velocity and the hematocrit (concentration of cells in the tube) in the organization of cells in a capillary. The precise role of the interplay between confinement and the cell deformability is still not fully elucidated.

It has been shown in a recent study that stable clusters of vesicles can form in the absence of bounding walls under an imposed parabolic flow profile [17]. Our objective in this paper is to take this unbounded case as a reference and see how confinement affects the hydrodynamic interactions. We generically find repulsion at short distance, and attraction at long distance. We also find that at a large enough vesicle interdistance the interaction can change sign, become repulsive, and then become attractive at higher interdistance. This points to the existence of an interaction which changes sign with distance, pointing to the nontrivial effect of hydrodynamic interactions. We further show that several branches of solutions can coexist, highlighting a complex imbricated interaction structure.

A systematic 2D numerical study (based on a boundary integral formulation) is undertaken here in order to analyze the evolution of a pair of vesicles, by exploring several parameters, such as channel width, initial interparticle spacing, and the flow strength. We then consider the case of a larger clusters of vesicles and show that the size of a stable cluster can be drastically modified by the presence of walls. Implication of the results to real situations is discussed. This paper is organized as follows. In Section II we introduce the model

in details. Section III presents the main results, for both weak and strong confinement. Section IV is devoted to a discussion of the results and the implication for real situations.

II. NUMERICAL FRAMEWORK

A. Membrane model

Vesicles, drops, capsules (drops coated with polymers) are endowed with different mechanical properties leading to different responses to external stresses. Both vesicles[18–21] and capsules[22–24] are widely used to mimic RBCs under flow. RBC’s complex dynamics, such as tank-treading, tumbling and vacillating breathing (aka swinging, trembling) can be reproduced by both vesicles and capsules. Other shapes exhibited by RBCs under a Poiseuille flow, such as parachute and slipper shapes, are also captured by the vesicle and capsule model (see review [25]). Vesicles resist bending, and possess an inextensible membrane (constant area in 3D and perimeter in 2D) but do not present a resistance to shearing, in contrast to RBCs and capsules, which are endowed with surface shear elasticity. Despite the absence of a cytoskeleton in the vesicle model several features exhibited by RBCs are also captured by vesicles, such as the above-mentioned dynamics and shapes under flow. The vesicle bending energy[26] is expressed in its two-dimensional form as

$$E_c = \frac{\kappa}{2} \oint c^2 ds + \oint \zeta ds, \quad (1)$$

where κ is the membrane bending modulus, c is the curvature, ds is the arclength element, and ζ is a Lagrange multiplier which enforces membrane inextensibility. The two-dimensional membrane force is obtained by calculating the functional derivative of the total energy

$$\mathbf{f}_{mem} = -\frac{\delta E}{\delta \mathbf{x}} = \kappa \left[\frac{\partial^2 c}{\partial s^2} + \frac{c^3}{2} \right] \mathbf{n} - c\zeta \mathbf{n} + \frac{\partial \zeta}{\partial s} \mathbf{t}, \quad (2)$$

where \mathbf{n} and \mathbf{t} are the outward normal and the tangent unit vectors, respectively. The details of the derivation can be found in Ref. [27]. The vesicle is characterized by its reduced area

$$\nu = \frac{S/\pi}{[p/(2\pi)]^2}, \quad (3)$$

a dimensionless parameter that expresses the ratio between the actual fluid area enclosed by the vesicle contour ($S = \pi R_v^2$) and the area of a disk having the same perimeter as the

vesicle. For a RBC, the reduced volume (3D equivalent of the reduced area) lies in the range of $0.60 - 0.65$. This will serve as a reference for our choice of parameter ν . The vesicle's equilibrium shape obtained by minimizing (1) for a reduced volume $\nu = 0.60 - 0.65$ is a biconcave shape similar to that exhibited by a RBC at rest [28].

B. Problem statement

1. Governing equations

It is convenient to decompose the total velocity $\mathbf{u}(u_1, u_2)$ into an undisturbed velocity in absence of vesicles $\mathbf{u}^\infty(u_1^\infty, u_2^\infty)$, and an induced velocity owing to the presence of vesicles $\mathbf{u}^D(u_1^D, u_2^D)$. This will help us to understand the interactions between vesicles (see section III). Here we consider a pressure-driven flow in a confined geometry between two laterally infinite plates (see Fig.1). The corresponding undisturbed velocity \mathbf{u}^∞ at a position $\mathbf{x}(x_1, x_2)$ is given by

$$\begin{cases} u_1^\infty(\mathbf{x}) = u_{max}[1 - (\frac{x_2}{W/2})^2] \\ u_2^\infty(\mathbf{x}) = 0, \end{cases} \quad (4)$$

where u_{max} is the midplane velocity and W is the channel width. The vesicles encapsulate an inner fluid with a viscosity (μ_{in}) and are suspended in an outer fluid with a viscosity (μ_{out}). For simplicity, we shall take $\mu_{in} = \mu_{out} = \mu$. The Reynolds number associated with a

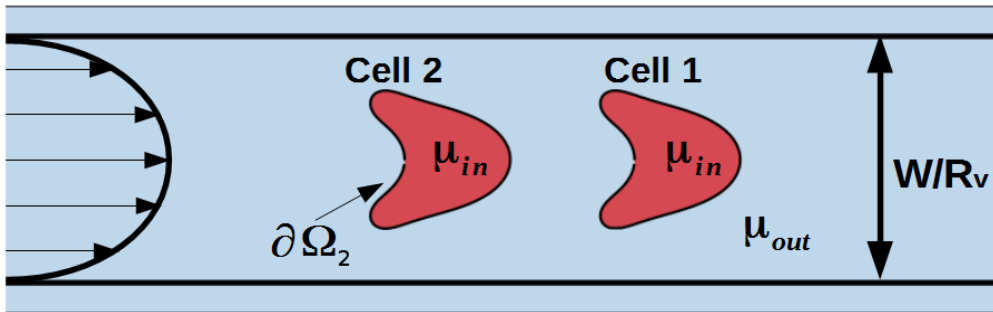


FIG. 1. Illustration of two vesicles driven by a Poiseuille flow and confined between two parallel walls situated at $x_2 = \pm W/2$.

vesicle (with typical size $10\mu m$, water viscosity and speed in the range of mm/s, as found in microcirculation) is of order 0.01. Thus fluid's motion can safely be described by the Stokes

equations

$$\nabla \cdot \sigma(\mathbf{x}) = -\nabla p(\mathbf{x}) + \mu \nabla^2 \mathbf{u}(\mathbf{x}) = 0, \quad (5)$$

$$\nabla \cdot \mathbf{u}(\mathbf{x}) = 0, \quad (6)$$

where σ is stress tensor associated to the total velocity and p is the pressure. The jump in the interfacial traction is balanced by the vesicle's membrane force $\mathbf{f}_{mem} = -[\sigma_{out} - \sigma_{in}]\mathbf{n}$. Besides the latter force balance condition, the solution of equations (5) and (6) must respect the following boundary conditions (B.C.)

$$\mathbf{u}(\mathbf{x}) = \mathbf{0}, \quad \text{when } \mathbf{x} \text{ lies on the walls} \quad (7)$$

$$\lim_{\mathbf{x} \rightarrow \infty} [\mathbf{u}(\mathbf{x}) - \mathbf{u}^\infty(\mathbf{x})] = \mathbf{0} \quad (8)$$

$$\mathbf{u}_{out}(\mathbf{x}) = \mathbf{u}_{in}(\mathbf{x}), \quad \mathbf{x} \in \partial\Omega_i \quad (i = 1, \dots, N_v) \quad (9)$$

2. Boundary integral formulation

The vesicles can be simply regarded as a collection of Lagrangian nodes advected by the flow. The motion of the vesicles is obtained by solving the advection equation for each material node \mathbf{x} lying on the membrane

$$\frac{d\mathbf{x}}{dt} = \mathbf{u}(\mathbf{x}) \quad (10)$$

The velocity of each membrane's discretization point can be deduced by solving an integral equation (discussed in what follows), and the position of each node is updated in time using an explicit Euler scheme.

$$\mathbf{x}(t + dt) = \mathbf{x}(t) + \mathbf{u}(\mathbf{x}(t), t)dt \quad (11)$$

In what follows we use dimensionless quantities defined as

$$c^* = cR_v, \quad \zeta^* = \zeta R_v^2/\kappa, \quad s^* = s/R_v, \quad \mathbf{u}^* = \mathbf{u}\tau_c/R_v,$$

$$\mathbf{x}^* = \mathbf{x}/R_v$$

where the relaxation time ($\tau_c = \frac{\mu R_v^3}{\kappa}$) and radius R_v of the vesicle are used as characteristic time and length scales. The dimensionless integral equation of the velocity along the membrane is given by

$$\mathbf{u}^*(\mathbf{x}^*) = \mathbf{u}^{\infty*}(\mathbf{x}^*) + \frac{1}{4\pi} \int_{\sum_i \partial\Omega_i} \mathbf{G}^{2W}(\mathbf{x}^*, \mathbf{y}^*) \mathbf{f}_{mem}^*(\mathbf{y}^*) ds^*(\mathbf{y}^*) \quad (12)$$

where $\mathbf{x}(x_1, x_2)$ and $\mathbf{y}(y_1, y_2)$ are two vector positions on the membrane. The integral in the RHS expresses the induced velocity owing to the vesicles. \mathbf{G}^{2W} is the Green's function associated with the Stokes equations and vanishes at the two bounding walls. The way this function is computed and its detailed expression are given in Refs. [29, 30].

The dimensionless expression of the membrane's force reads

$$\mathbf{f}_{mem}^* = \frac{1}{C_a} \left\{ \left[\frac{\partial^2 c^*}{\partial s^{*2}} + \frac{c^{*3}}{2} \right] \mathbf{n} - c^* \zeta^* \mathbf{n} + \frac{\partial \zeta^*}{\partial s^*} \mathbf{t} \right\} \quad (13)$$

In addition to the vesicle reduced area defined above ($\nu = (S/\pi)/(p/2\pi)^2$), and the confinement given by $C_n = \frac{2R_v}{W}$, we have a new dimensionless number associated to the flow in equation (12), which is given by

$$C_a = \frac{\mu R_v^3 \dot{\gamma}}{\kappa} = \frac{\mu R_v^3 u_{max} R_v}{\kappa (W/2)^2}. \quad (14)$$

We will refer to this number as the capillary number, where $\dot{\gamma} = R_v u_{max}/(W/2)^2$ is the shear rate defined at $x_2 = R_v/2$. We recall that the shear rate in a parabolic flow is not a constant unlike in a shear flow. Thus, the definition of the capillary number for a parabolic flow is not unique in the literature. The capillary number is the ratio between the flow stress and bending force density. It may be viewed also as the ratio between the characteristic shape relaxation time $\tau_c = \mu R_v^3/\kappa$ and the time scale of the flow $\tau_f = 1/\dot{\gamma}$. In order to have an idea on the conversion of dimensionless units into physical ones, the following dimensional numbers can be used: $R_v = 3\mu m$, $\mu = 10^{-3}$ Pa.s and $\kappa = 10^{-19} J$. This leads to a characteristic time of relaxation of the cell of about $\tau_c \sim 0.2 - 0.3$ s. This is quite consistent with measured values for RBCs[31, 32].

III. RESULTS

In this section, simulations of a pair of vesicles in channels of different widths are performed. The vesicles are initialized as ellipses elongated in the direction of the flow, if not stated otherwise. The pair interdistance, a quantity that will be used to quantify the interaction between vesicles, is measured between the mass centers of adjacent vesicles. We will also investigate the role of the capillary number, and the impact of initial conditions (shapes and interdistances) on the final state. We shall see that there are several coexisting solutions.

A. Weak confinement

A previous study has been devoted to the cluster formation in the absence of walls [17]. We first study the evolution of a pair of vesicles in a weak confinement in order to check that we can capture almost the same result. We have analyzed the evolution of a pair of vesicles in a channel having a width $W = 20R_v$, which corresponds to a weak enough confinement. We find that the final equilibrium distance is equal to about $2.53R_v$ for $W = 20R_v$. This result compares well with that obtained in unbounded flow [17] where the final distance is of about $2.4R_v$.

We have analyzed systematically the behavior of a pair of vesicles for different confinements (but still weak enough confinement) and different initial conditions. Figure 2 shows a typical evolution of the pair interdistance as a function of time for different initial conditions, denoted as d_{init} in that figure. We see there that different initial conditions lead to the same final state.

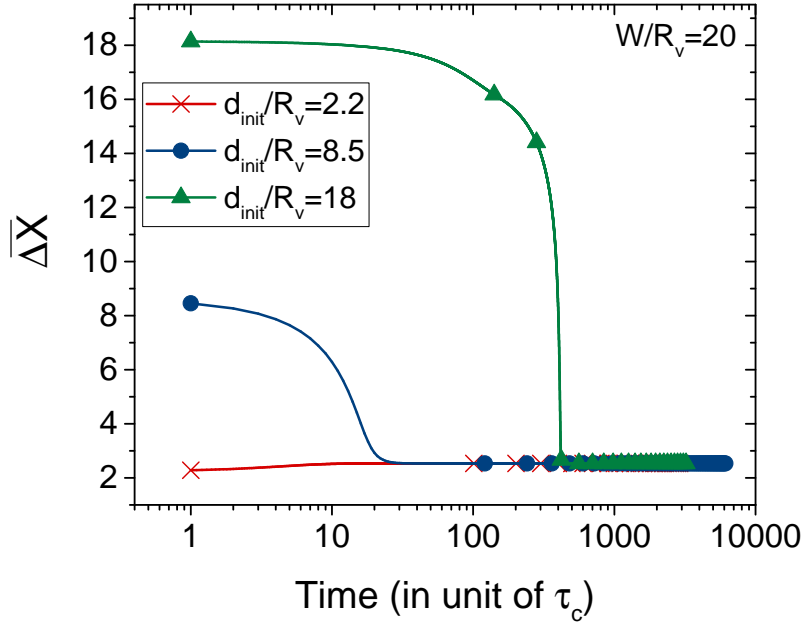


FIG. 2. The pair interdistance as a function of time for different initial conditions (initial interparticle spacing). $W = 20R_v$, and $C_a = 10$. Note that the x-axis is represented in semilog scale.

Figure 3 shows the final configuration of the pair of vesicles as well as the induced flow field, that is the total flow field from which we subtract the imposed Poiseuille flow (as

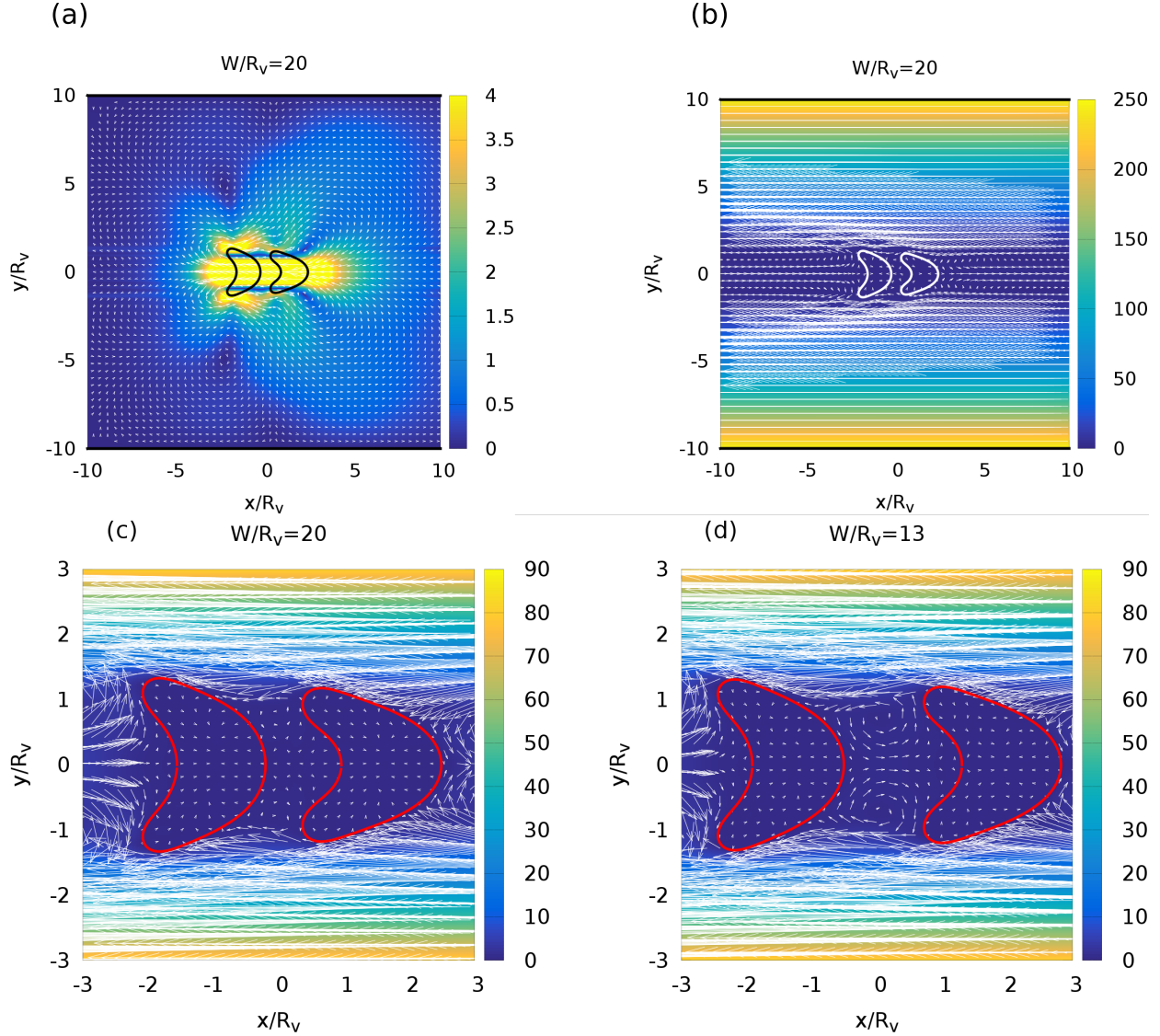


FIG. 3. The induced flow field for a pair of vesicles in a weakly confined flow (a); $W = 20R_v$. We also represent the flow in the frame moving with the vesicle called hereafter “comoving frame” (b). A zoom in the comoving frame in the region located between the cells reveals the absence of bolus in case of $W = 20R_v$ where the final interdistance is about $2.4R_v$ (c); and the presence of quasi-circular bolus for $W = 13R_v$ where the final interdistance is of about $3.4R_v$ (d).

defined in section II B 1). This figure also shows the total flow field. It can be seen that the induced flow ahead of the leading vesicle (the one on the right) is converging towards the vesicle. This means that if a tracer is placed ahead of the leading vesicle it will be attracted by that vesicle. This qualitatively hints to the fact that the vesicle would attract small objects placed ahead of it. The qualitative understanding of this flow field is quite simple,

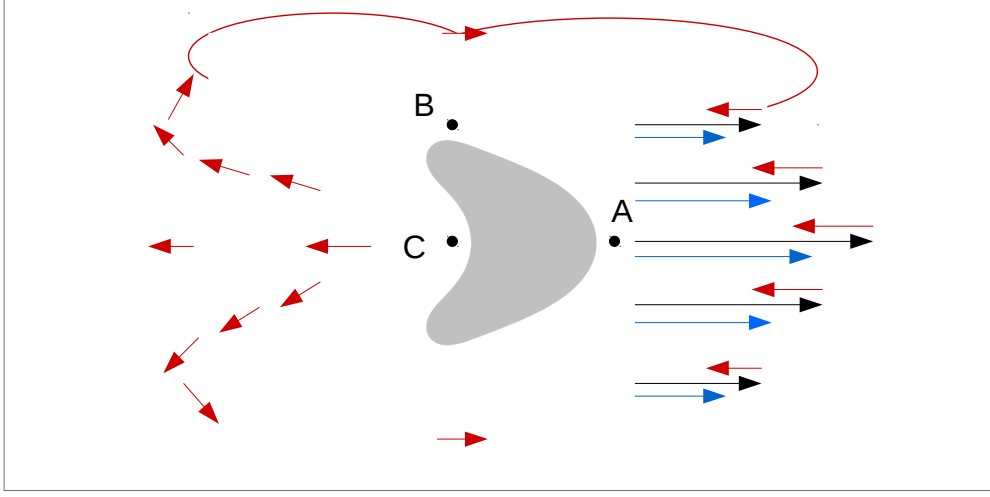


FIG. 4. A schematic explanation of the flow field around a vesicle in a confined Poiseuille flow. The black, red and blue arrows represent, respectively, the unperturbed, disturbed and total velocity fields. The capillary number and the channel's width are $C_a = 10$ and $W = 8R_v$.

as shown schematically in Figure 4. We show there the imposed flow (black arrows), the total flow (blue) and the induced flow (red). Consider the flow field ahead of the vesicle at the center line. Far away from the vesicle the total flow field practically coincides with the imposed one (the perturbation due to the vesicle decays away from the vesicle). Consider now a point close enough ahead of the vesicle (point A in the Figure). The vesicle moves with a velocity which is smaller than the maximum imposed velocity, so that close enough to the vesicle (due to velocity continuity), the full velocity of the fluid ahead of the vesicle is smaller than the maximum imposed one (the blue arrow is shorter than the black one). If we consider the induced flow only (which is what matters for interaction), we have to subtract the black arrows (imposed flow) from the blue ones (the full field), so that at the center line ahead of the vesicle the induced flow (red arrows) points towards the vesicle. The same reasoning applies to the rear part of the vesicle (point C), meaning that the induced flow is directed away from the vesicle. Consider now a point on the side part of the vesicle (point B in the figure). Since the vesicle is at the center its velocity is higher than that of the adjacent fluid near on top of point B . At point B , because of velocity continuity, the vesicle and the fluid move at the same velocity, which is higher than the imposed flow at that point. Subtracting the imposed flow from the total flow field around point B shows that the flow field there point to the right. Joining now point A , B and C (see Figure 4), we

obtain the qualitative pattern for the induced flow field where the flow goes from the rear to the front of the vesicle.

In order to analyze further this question we have systematically analyzed in details the behavior of the relative velocity of the two centers of mass of the pair of vesicles as a function of their actual interdistance by considering different initial interdistances. Let us denote the leading vesicle by 1 and the following vesicle by 2, and let $X_1(t)$ and $X_2(t)$ denote their instantaneous positions, and by V_1 and V_2 the corresponding velocities (velocity of center of mass has only a component along the wall direction). Their relative velocity is given by $\Delta V \equiv V_1 - V_2$. A positive value of ΔV means that the two vesicles repel each other, while a negative value means they attract each other. An equilibrium position corresponds to $\Delta V = 0$. In what follows we will refer to the dimensionless velocity, defined as $\overline{\Delta V} = \Delta V / (R_v / \tau_c)$. Figure 5 shows $\overline{\Delta V}$ as a function of the dimensionless interdistance

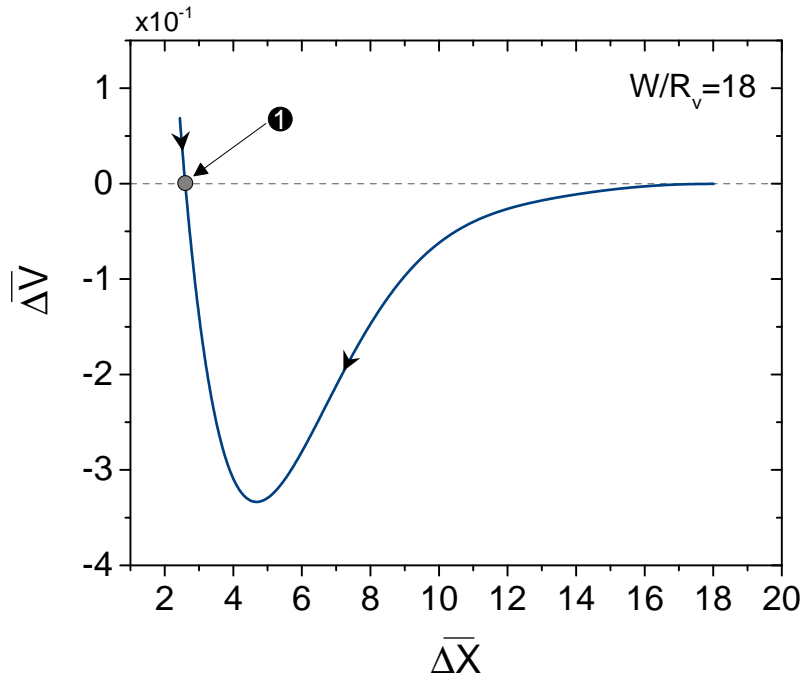


FIG. 5. The relative velocity as a function of the relative distance; $W = 18R_v$, and $C_a = 10$.

between centers of mass, $\overline{\Delta X} \equiv (X_1 - X_2)/R_v$. We observe a repulsion at short distance and an attraction at long distance. There is a final equilibrium position characterized by $\overline{\Delta V} = 0$ (denoted as 1 within a dark circle in Figure 5). This equilibrium position is unique, independent from the choice of the initial shape (Figure 6).

This defines in a non ambiguous way the equilibrium position. Clearly, that equilibrium

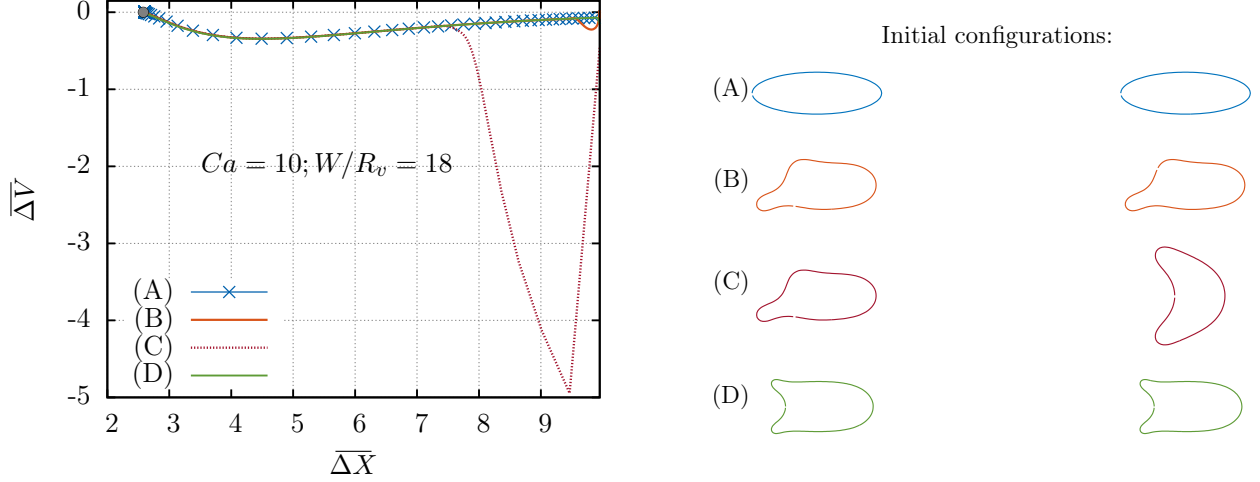


FIG. 6. The relative velocity as a function of the relative distance; $W = 18R_v$, and $Ca = 10$. Starting from different initial shapes, the pair of vesicles converges to the same equilibrium interdistance. The labels (A), (B), (C), and (D) corresponds to the initial shapes depicted in right figure.

point is stable, since for higher interdistance the relative velocity is negative, so that the vesicles will attract each other, while the opposite happens for smaller interdistance. Generally, if the relative velocity crosses zero (when ΔX increases) from positive to negative values the equilibrium position is stable, and is unstable otherwise.

We have performed this study for several confinements, but still weak enough, and have determined the corresponding equilibrium position. Figure 7 shows the branch of equilibrium interdistance $\Delta \bar{X}$ as a function of W/R_v . The equilibrium interdistance weakly depends on confinement, and remains close to about $3R_v$.

B. Strong confinement

Let us now examine the generic behavior for a strong confinement. Consider the case $W = 3R_v$. By studying the evolution of the interdistance as a function of time, we find that for several initial conditions the pair of vesicles finally settles into a bound and stable steady state. Figure 8 shows the evolution of the interdistance with time for different initial conditions. The first noticeable fact is that the equilibrium distance for $W = 3R_v$ is significantly larger than that obtained at weak confinement. For example for $W = 3R_v$ the equilibrium interdistance is about $5R_v$, which is twice as large as that obtained in the weak

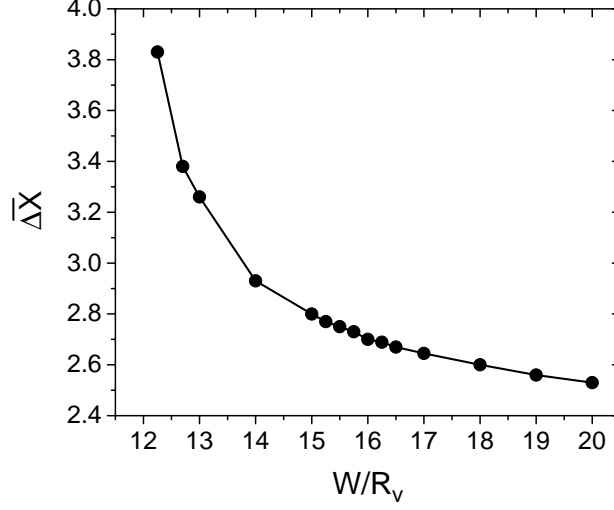


FIG. 7. The branch of solution representing the equilibrium interdistance as a function of the channel width.

confinement case (about $2.5R_v$). A first interpretation would be that the presence of the walls screens the hydrodynamics interaction. This reasoning is, *a priori*, not justified, since the screening concerns both the attraction and repulsion and it is not clear how would the confinement shift the attraction and repulsion zones.

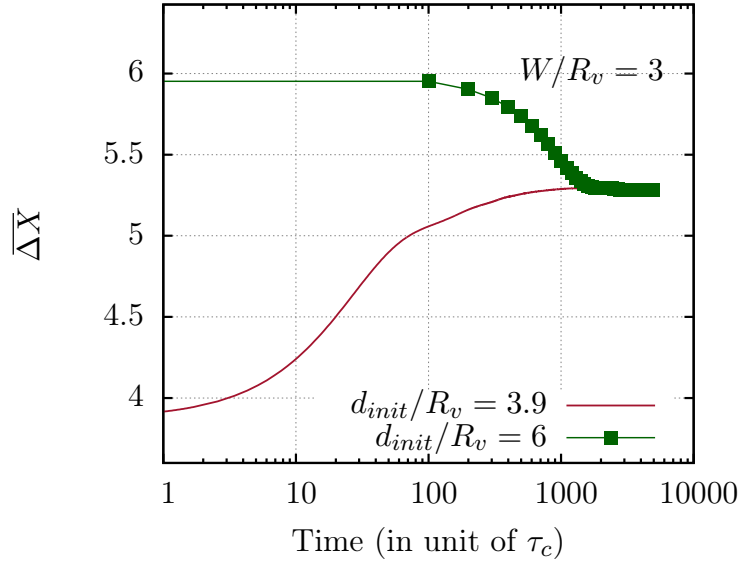


FIG. 8. The pair interdistance as a function of time (shown here in a semi-log scale) for different initial conditions. $W = 3R_v$, $C_a = 10$.

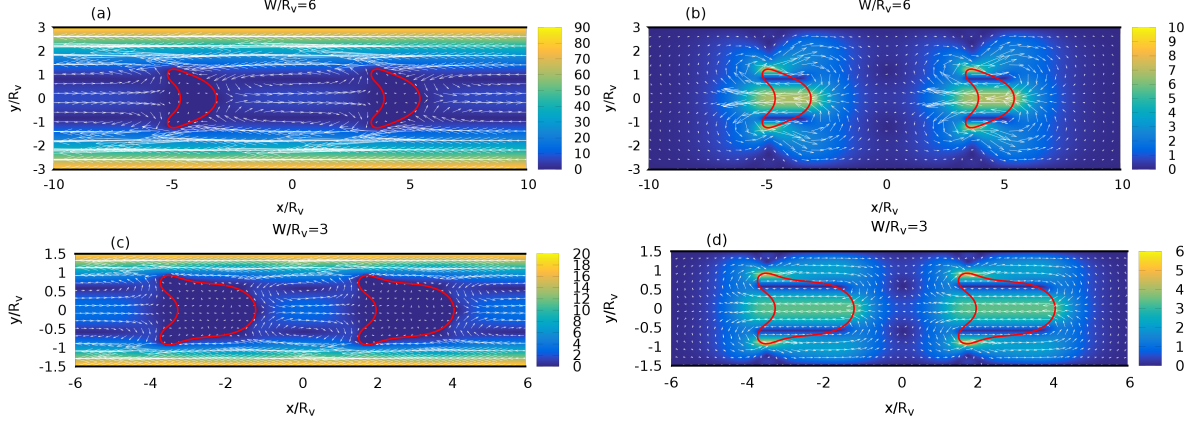


FIG. 9. The flow field in a comoving frame (a,c) and the induced flow (b,d) field for a pair of vesicles for $W = 6R_v$ and $W = 3R_v$.

Let us first analyze the velocity field in a strong enough confinement regime. Figure 9 shows the induced flow field for two confinements $W = 6R_v$ and $W = 3R_v$. We also show there the flow field in the co-moving frame (the frame moving with the pair). The main difference with the weak confinement is the fact that the flow lines, which extend far away in the weak confinement (see Figure 3), are cut-off by confinement in the strong confinement case. This partially hints to a weaker interaction in magnitude, as we shall see below.

As done above for the weak confinement case, we have analyzed the relative velocity as a function of the relative distance. A typical result is shown in Figure 10. We obtain a

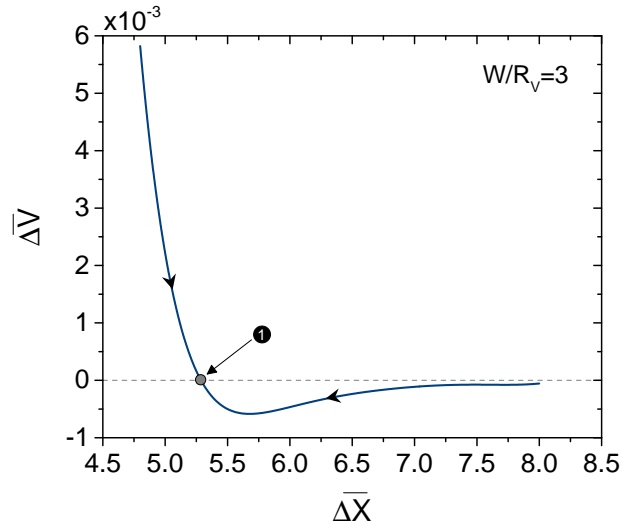


FIG. 10. The relative velocity as a function of the relative distance; $W = 3R_v$, and $C_a = 10$.

stable equilibrium position, with short-range repulsion and long-range attraction. We find that the relative velocity amplitude is significantly smaller than that obtained for a weak confinement (compare with Figure 5). This is to be traced back to the screening effect due to the walls that weakens the interaction.

We have performed this study for several confinements, and have determined the equilibrium position. Figure 11 shows the branch of equilibrium position $\overline{\Delta X}$ as a function of

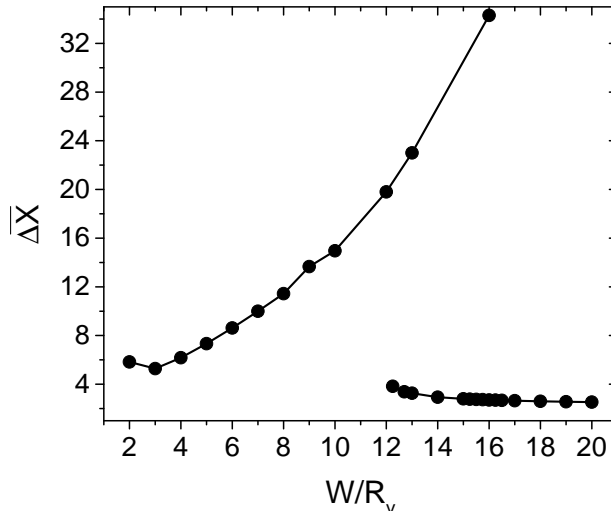


FIG. 11. The branch of solution representing the equilibrium interdistance as a function of the channel width for a strong enough confinement.

W/R_v . In contrast to the weakly confined case (also shown in Figure 11) the equilibrium distance strongly depends on confinement, and varies from about $4R_v$ up to about $32R_v$. Some remarks are in order. We have a new branch of solution for small values of W (the left branch in Figure 11), different from that discussed above for large W (the right branch in Figure 11). The second observation is that we have two distinct branches, one presents an equilibrium distance which increases with W , while the other has an equilibrium position which decreases with W .

C. Complex phase diagram

We have made further studies in order to clarify the overall structure of the topology of the phase diagram. First, we have tried to analyze the basin of attraction of the branches by exploring a wider range of initial conditions. We begin our discussion with the weak

confinement case (large W). We have already seen in the previous section that different initial conditions lead to the same final solution. By exploring wider and wider regions of initial conditions, we have found a different scenario. By keeping the same confinement $W = 13R_v$, as done above, we found that beyond a certain initial pair interdistance, the solution does not evolve anymore to the previous solution, but rather to another solution. Figure 12(left) shows the temporal evolution where after $25000\tau_c$ the pair interdistance is

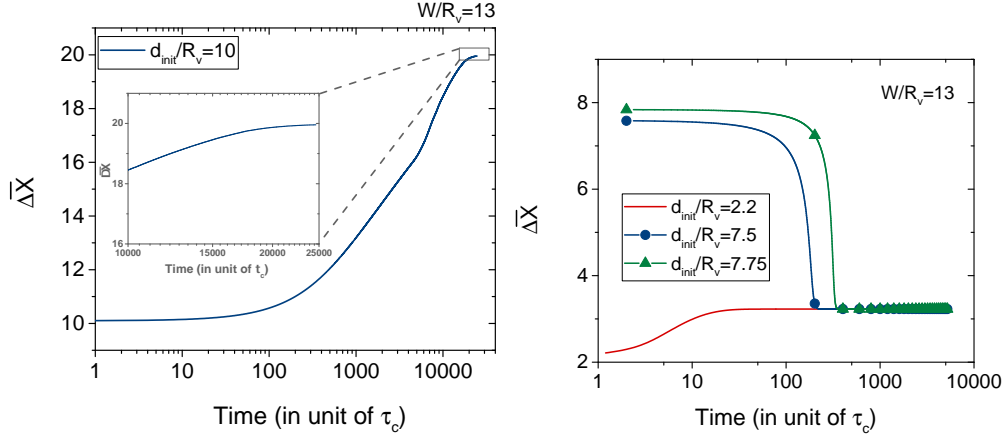


FIG. 12. The pair interdistance as a function of time for different initial interparticle spacing: $d_{init}/R_v = 10$ (left); and 2.2, 7.5, and 7.75 (right). $C_a = 10$ and $W/R_v = 13$. Note that the x-axis is represented in semilog scale.

still evolving, but converges ultimately to a distance of about $23R_v$. For different initial conditions (smaller initial interdistance) we found before a final distance of about $3.4R_v$ (Figure 12(right)). This clearly shows the coexistence of two different stable solutions. In general, these two stable solutions should be separated by an unstable solution. Therefore, we need to determine the location of the unstable branch. We can have access to this by analyzing the relative velocity as a function of interdistance (as performed before). Figure 13 shows the result, where the points denoted as 1, 2 and 3 in the figure, refer to the location where the pair relative velocity vanishes. Since the relative velocity around point '3' is very small, we have made a zoom in order to reveal the structure of the evolution of the relative velocity. Points 1 and 3 are stable, whereas point 2 is unstable.

We have made a systematic analysis of this kind by varying the confinement (i.e. W) in order to build the full diagram representing the equilibrium solutions (like point 1, 2 and 3) as a function of W . The results are summarized in Figure 14. We see that the

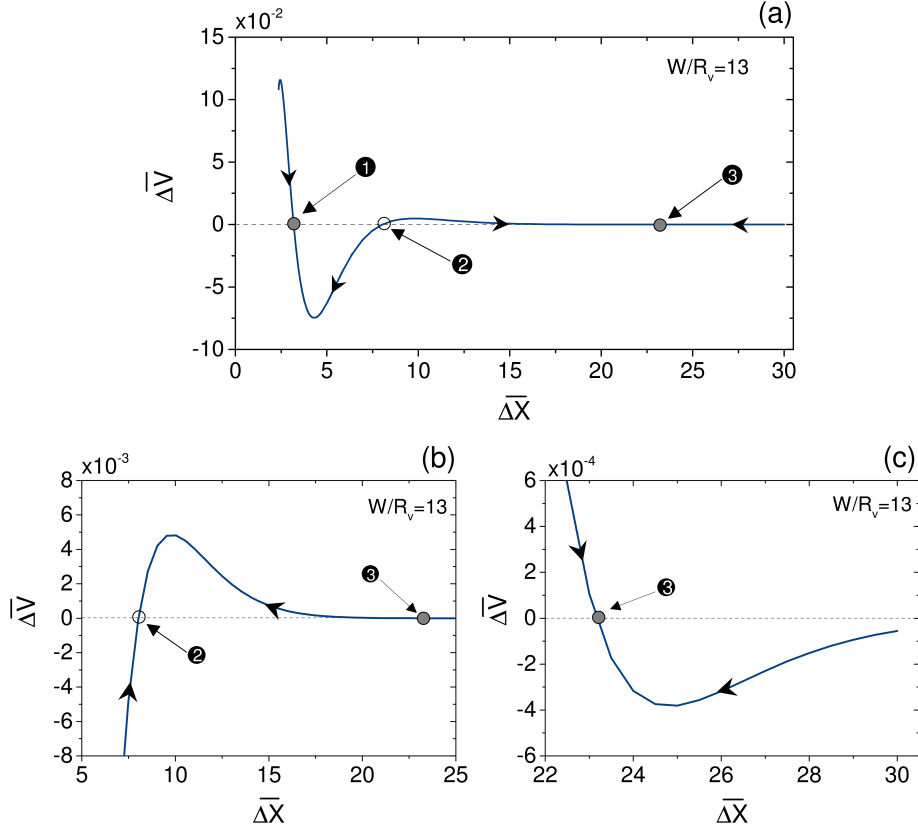


FIG. 13. Normalized relative velocity as a function of the interparticle spacing for $W/R_v = 13$. (a), (b) and (c) show successive zooms. Solid dots and open circles represent, respectively, stable and unstable fixed points. A succession of stable and unstable fixed points is observed.

branch for high W undergoes a fold singularity in the form of a saddle-node bifurcation, where a stable solution (represented by solid line) merges with an unstable solution (dashed line). The branch arising at low W continues to exist (as a stable solution) beyond the saddle-node point, and does not show, for the values of W explored so far, any tendency of disappearance. Theoretically, this branch either continues to exist for any W , or may undergo a fold singularity, which is one of the scenario expected from catastrophe theory. Since for large W the relative velocity is too small, the question of the behavior of the branch at large enough W has only an academic interest. We shall thus not dwell further on this issue here.

Finally, let us say few words on the strength of interaction as a function of confinement. As can be expected, the confinement reduces the strength of interaction, due to screening.

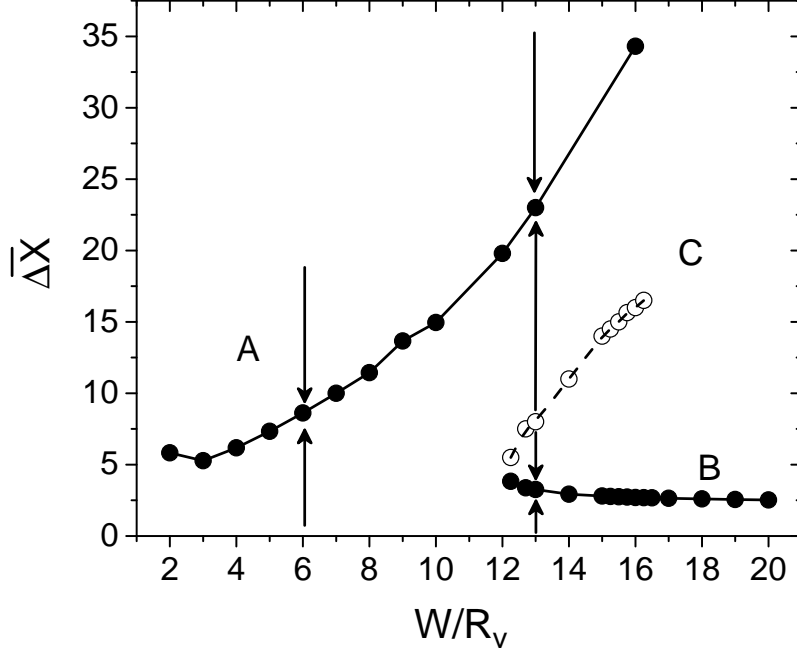


FIG. 14. The full set of branches of solution representing the equilibrium interdistance as a function of the channel width. Solid lines represent stable branches whereas dashed lines unstable branches.

To understand the difference of the pairing mechanism at large and small channel widths we first consider a pair of vesicles in two different channels of width $6R_v$ and $15.25R_v$. The time evolution of the interdistances in each channel is shown in Figure 15. The time needed

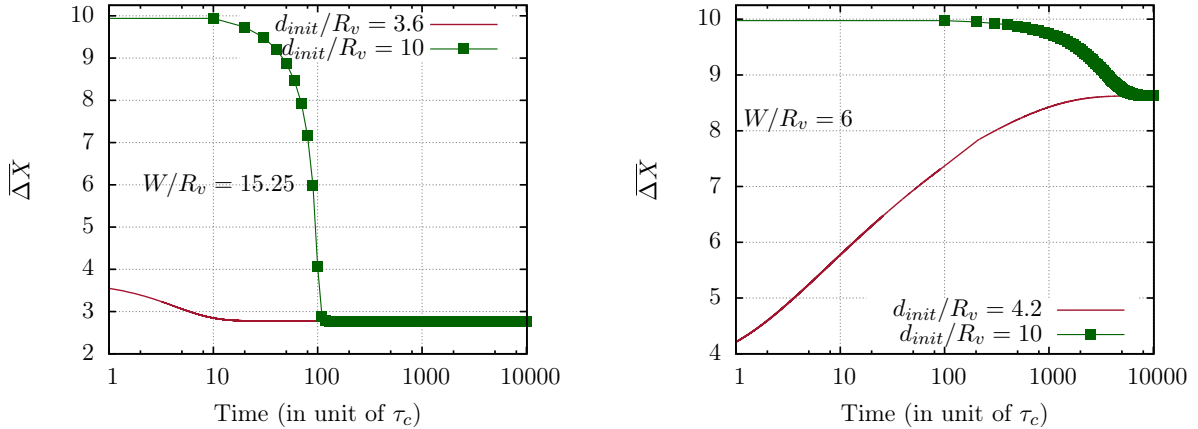


FIG. 15. Time evolution of the interparticle spacing between two vesicles in different channel widths. (a) $W = 15.25R_v$. (b) $W = 6R_v$. Two initial interdistances were used $d_{init} = 3.7$ and $10R_v$, respectively. Note that the x-axis is represented in semilog scale.

to reach the steady state for different channel widths has been investigated. We found that

their interdistance reduces by approximatively $1.4R_v$ the pair of vesicles needs around $7000\tau_c$ in a channel of width $W = 6R_v$ whereas only $120\tau_c$ are needed to reduce their interdistance by $7.2R_v$ in a channel of width $W = 15.25R_v$. Since a typical time τ_c for RBC is about 0.1 s, this gives about 10 s in the first case. Note also that in reality there are always fluctuations and imperfection so that the cells are not all at the same lateral position. For example, if the leading cell is slightly off-centered its velocity may be sensibly different from the following cell, so that the time needed to reach the bound state may occur at a significantly shorter time scale than 10 s.

D. Effect of the capillary number

In this section we describe the effect of the capillary number on the main results. We consider a pair of cells with four different capillary numbers $Ca = \{5, 10, 25, 100\}$ and flowing in channels of width ranging from $2R_v$ to $20R_v$ (≈ 6 to $60 \mu m$ for RBCs). Figure 16 depicts the stationary interparticle spacing as a function of the channel width for different capillary numbers (we do not show the full branch as before due to computational cost, and especially because we do not see any significant changes). The stationary shape of the vesicles at high confinement ($W/R_v \leq 3$) is asymmetric for $Ca \leq 25$. The shape asymmetry decreases with the increase of the capillary number and a transition from asymmetric to symmetric shapes is observed at $Ca = 100$ (Figure 16 (b)). The shapes become fully symmetric for a channel width $W/R_v \geq 4$ and the final pair interdistance tend to the same value, independent from the capillary number. For $Ca \geq 10$ the choice of the initial shapes does not affect the stationary solution whereas for $Ca < 10$ it leads to two different solutions in the region of transition resulting in a decrease of the stationary interdistance if starting with parachutes and the opposite if starting with ellipses. (Figure 16 (c) and (d)). The time needed to reach the stationary shape is proportional to the capillary number (higher Ca is shorter the time needed to transform an ellipse to a parachute) which explains the dependency on the initial shapes at low Ca . Globally, the capillary number seems to not significantly affect the behavior of the pair. For vesicles, higher values of Ca can be reasonably reached, such as 2000. For a vesicle of radius $20 \mu m$, a channel radius of $200 \mu m$, and a velocity of $1 cm/s$, one finds approximately $Ca \simeq 1600$. By assuming that the relative velocity scale with Ca (as shown in Figure 17), one finds that the relative velocity is of about $100R_v/\tau \sim 1R_v/s$,

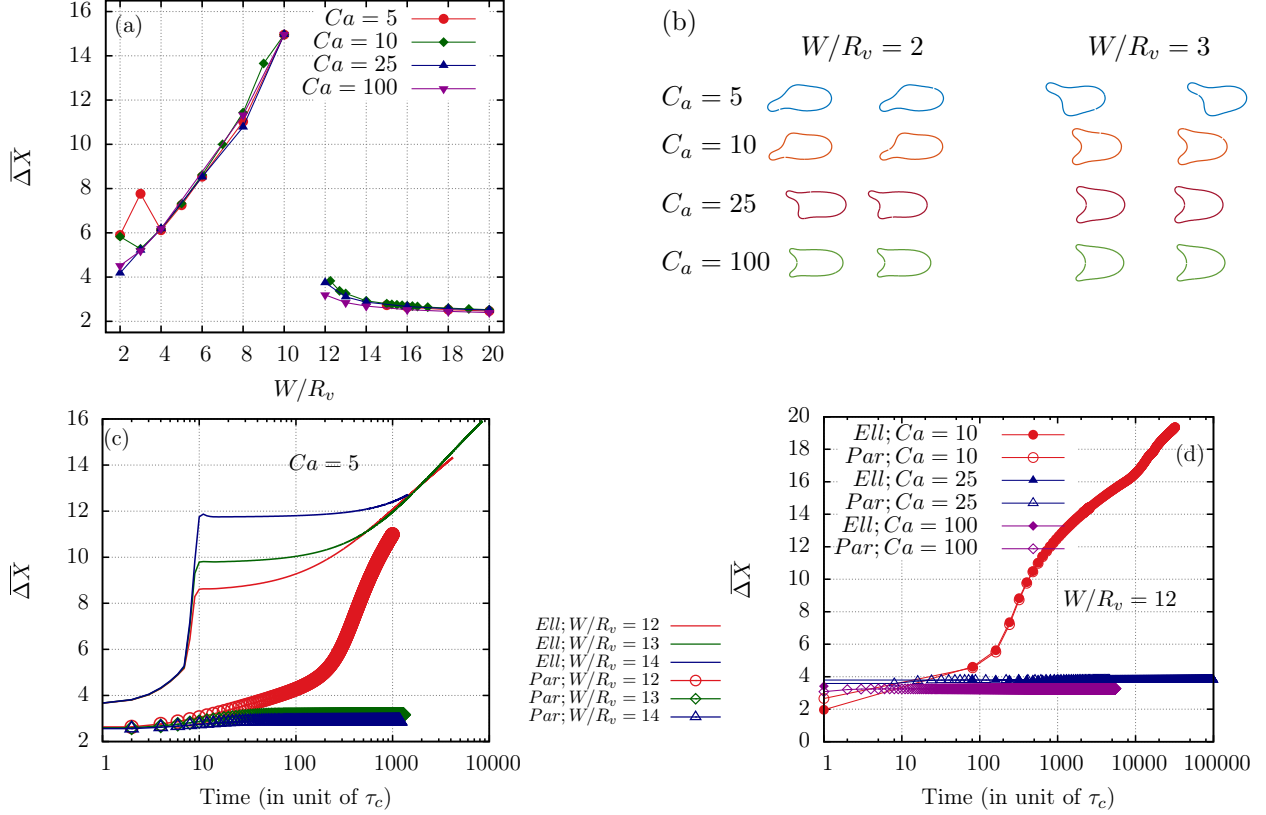


FIG. 16. Stationary interparticle spacing as function of the channel width for different capillary numbers (a). The stationary shapes for different capillary number at high confinement $W/R_v = 2$ and 3 (b). Role of the initial shape (solid lines are ellipses “Ell” and dashed lines are parachutes “Par”) on the time evolution of the pair interdistance for $Ca = 5$ and $W/R_v = 12, 13$ and 14 corresponding to the transition area (c). Same as (c) but for $W/R_v = 12$ and $Ca = 10, 25$, and 100 (d).

which is no devoid of experimental testability.

E. Larger cluster formation

The above study has focused on the case of a pair of vesicles. The question thus arises of whether this would allow us to draw some general conclusion about the size of clusters when more cells are present. The situation is quite complex, and here we only quote some basic examples leaving a systematic study to the future. In a recent work [17] it has been reported that, in an unconfined Poiseuille flow, the cluster size depends on the flow strength: a higher

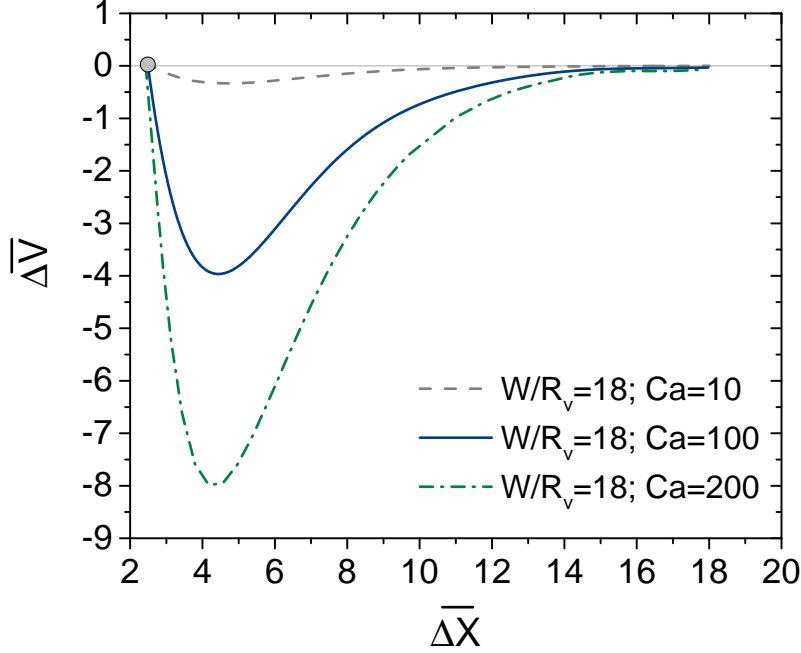


FIG. 17. Relative velocity as a function of interdistance in a weak confinement $W/R_v = 18$ for different capillary numbers. The dashed (grey), solid (blue), and dash-dotted (green) lines are for $Ca = 10$, 100 , and 200 , respectively.

flow strength leads to a larger cluster size. While this tendency is confirmed here, we find that even for a large enough W (about $20R_v$) where the confinement might be considered as weak, we obtain some important differences with the unconfined case [17]. We have considered the largest Ca explored in [17] ($Ca = 10$), and for which it has been reported that the largest stable cluster contains 10 cells (for a reduced area $\nu = 0.65$). We have investigated here the largest stable cluster in the presence of a weak confinement. Figure 18 shows different initial configurations of parachute-like cells initialized as clusters of different sizes and their corresponding final state. It is seen that for $W = 20R_v$, the cluster is stable as long as the number of cells is smaller than, or equal to, 4. Beyond $N_v = 4$, the leading cells detach progressively one after the other from the initial cluster with a variable time gap until decreasing the number of cells within the cluster down to 4 (see the Movies in the Supplementary Material). The maximum size of a stable cluster obtained in unconfined flow was $N_v = 10$, whereas here we obtain $N_v = 4$ in a weakly confined flow corresponding to $W = 20R_v$ ($\equiv C_n = 0.1$). This clearly means that the confinement, despite being weak, alters significantly the results. In a future study we plan to analyze in detail the dependence



FIG. 18. Different initial configurations (left) and final configurations (right) of clusters of different sizes flowing in a channel of width $W/R_v = 20$.

of the largest stable cluster size on the confinement.

IV. CONCLUSION

This study has reported on a complex phase diagram regarding hydrodynamic interaction between two vesicles in a confined pressure-driven flow. It is found that several branches of stationary solutions coexist. It would be interesting in the future to extend this study to the three-dimensional case both for vesicles and RBCs. Another important ingredient is to analyze the interplay between hydrodynamic interaction and that due to plasma proteins and study how the structure of the phase diagram reported here evolves in this case. Another interesting task for future investigations is to study collective behaviors when many cells are present and determine the link between the spatio-temporal organization and the rheology.

ACKNOWLEDGMENTS

We acknowledge financial support from the German Science Foundation research initiative SFB1027, the German French University (DFH/UFA), CNES (Centre d'Etudes Spatiales)

and ESA (European Space Agency).

- [1] R. Skalak and P. I. Branemark, *Science* **164**, 717 (1969).
- [2] P. Gaehtgens and H. Schmid-Schönbein, *Naturwissenschaften* **69**, 294 (1982).
- [3] G. Tomaiuolo, L. Lanotte, G. Ghigliotti, C. Misbah, and S. Guido, *Physics of Fluids* (1994-present) **24**, 051903 (2012).
- [4] M. Brust, O. Aouane, M. Thiébaud, D. Flormann, C. Verdier, L. Kaestner, M. Laschke, H. Selmi, A. Benyoussef, T. Podgorski, *et al.*, *Scientific reports* **4** (2014).
- [5] H. Wang and R. Skalak, *Journal of Fluid Mechanics* **38**, 75 (1969).
- [6] S. Leichtberg, R. Pfeffer, and S. Weinbaum, *International Journal of Multiphase Flow* **3**, 147 (1976).
- [7] B. Cui, H. Diamant, and B. Lin, *Phys. Rev. Lett.* **89**, 188302 (2002).
- [8] B. Cui, H. Diamant, B. Lin, and S.A. Rice, *Phys. Rev. Lett.* **92**, 258301 (2004).
- [9] H. Diamant, B. Cui, B. Lin, and S. Rice, *Journal of Physics: Condensed Matter* **17**, S2787 (2005).
- [10] T. Beatus, T. Tlustý, and R. Bar-Ziv, *Nature Physics* **2**, 743 (2006).
- [11] T. Beatus, R. Bar-Ziv, and T. Tlustý, *Physical review letters* **99**, 124502 (2007).
- [12] I. Shani, T. Beatus, R. H. Bar-Ziv, and T. Tlustý, *Nature Physics* **10**, 140 (2014).
- [13] P. Janssen, M. Baron, P. Anderson, J. Blawdziewicz, M. Loewenberg, and E. Wajnryb, *Soft Matter* **8**, 7495 (2012).
- [14] J. L. McWhirter, H. Noguchi, and G. Gompper, *Proceedings of the National Academy of Sciences* **106**, 6039 (2009).
- [15] M. Thiébaud, Z. Shen, J. Harting, and C. Misbah, *Physical Review Letters* **112**, 238304 (2014).
- [16] J. McWhirter, H. Noguchi, and G. Gompper, *Soft Matter* **7**, 10967 (2011).
- [17] G. Ghigliotti, H. Selmi, L. E. Asmi, and C. Misbah, *Physics of Fluids* (1994-present) **24**, 101901 (2012).
- [18] C. Misbah, *Phys. Rev. Lett.* **96**, 028104 (2006).
- [19] H. Noguchi and G. Gompper, *Physical review letters* **98**, 128103 (2007).
- [20] A. Farutin, O. Aouane, and C. Misbah, *Physical Review E* **85**, 061922 (2012).

- [21] O. Aouane, M. Thiébaud, A. Benyoussef, C. Wagner, and C. Misbah, Phys. Rev. E **90**, 033011 (2014).
- [22] S. Ramanujan and C. Pozrikidis, Journal of Fluid Mechanics **361**, 117 (1998).
- [23] E. Lac and D. Barthès-Biesel, Physics of Fluids (1994-present) **17**, 072105 (2005).
- [24] S. Kessler, R. Finken, and U. Seifert, Journal of Fluid Mechanics **605**, 207 (2008).
- [25] P. M. Vlahovska, D. Barthes-Biesel, and C. Misbah, Comptes Rendus Physique **14**, 451 (2013), living fluids / Fluides vivants.
- [26] W. Helfrich, Z. Naturforsch. **28c**, 693 (1973).
- [27] B. Kaoui, G. H. Ristow, I. Cantat, C. Misbah, and W. Zimmermann, Phys. Rev. E **77**, 021903 (2008).
- [28] P. Canham, Journal of Theoretical Biology **26**, 61 (1970).
- [29] C. Pozrikidis, *Boundary Integral and Singularity Methods for Linearized Viscous Flow*, Cambridge Texts in Applied Mathematics (Cambridge University Press, 1992).
- [30] M. Thiébaud and C. Misbah, Phys. Rev. E **88**, 062707 (2013).
- [31] R. Hochmuth, P. Worthy, and E. Evans, Biophysical journal **26**, 101 (1979).
- [32] G. Tomaiuolo and S. Guido, Microvascular research **82**, 35 (2011).